Wave-packet model for excitation by ultrashort pulses

Kalle-Antti Suominen, Barry M. Garraway, and Stig Stenholm
University of Helsinki, Research Institute for Theoretical Physics, Siltavuorenpenger 20 C, 00170 Helsinki, Finland
(Received 13 September 1991)

In this paper we discuss the excitation of a localized molecular ground-state wave function by a short laser pulse. With a one-dimensional approach we show when it is possible to excite a considerable fraction of the ground state without too much distortion of the shape of the wave packet. This is of interest in time-resolved molecular experiments where an excited wave packet is often taken as the initial state. We solve the two coupled wave equations numerically and compare results to an analytical approximation based on the Rosen-Zener model. The validity of the approximation and its breakdown is considered in detail. Special attention is paid to the effect of lengthening the pulse duration and the consequences of the accompanying number of Rabi flops occurring in the area theorem. When the approximation breaks down, the wave packet becomes distorted and spread out, but there are still interesting coherence effects due to the interplay between the Rabi flopping and the molecular dynamics; these are displayed and discussed. Finally, the relationship to other works and possible generalizations are presented.

PACS number(s): 33.80.Be, 03.65.Bz

I. INTRODUCTION

The modern development of technology for ultrashort laser pulses has made it possible to study fast phenomena in atoms, molecules, and solids in real time. Experimentalists can now excite and probe microscopic degrees of freedom over time scales that exhibit characteristics of genuine quantum evolution. On the theoretical side, modern computers and advanced numerical methods allow the integration of models that contain the main features of real atomic systems investigated experimentally. Thus, one can follow the genuine time dependence of quantum-mechanical systems in situations not usually discussed in the conventional applications of quantum mechanics.

In our previous investigation [1], we have discussed the time evolution of wave packets on crossing excited-state potential surfaces; see Refs. [2–4], and references therein. Formulating the molecular energy-level structure in terms of Born-Oppenheimer potentials [1], we can treat the wave packets with a model of coupled-channel wave functions on different electronic-potential surfaces. In [1] and [5], we assumed that the excited wave packet started its motion on one potential and was transferred to another one at a laser-induced level crossing. We compared the results of exact numerical investigations of the wave-packet motion with those obtained from the well-known Landau-Zener approximation for the level crossings.

In our earlier work we also assumed that the ground-state wave function could be excited to an upper-potential surface without too much distortion; this is the assumption of adiabatic excitation. In this way we could obtain a well-localized wave packet as the initial state for our level-crossing calculations. It is, however, important to know the conditions and circumstances which make it possible to lift the well-localized ground state to an excited level without significant distortion. This is the problem investigated in the present paper.

In perturbation theory, the shape of the ground-state wave function is transferred to the excited state unchanged, but in this case only a minor fraction of the population can be excited. With an increase in laser intensity, it becomes possible to achieve larger excitation, which is also desirable from an experimentalist's point of view. For certain pulses, so-called π pulses, all the population becomes excited, and one may ask if this is achievable without distortion of the wave packet. On the other hand, an increase in laser intensity may return population to the lower level, and a 2π pulse leaves the level populations unchanged. What is the behavior of the wave packet in such cases?

We also know that a very short exciting pulse can be approximated by a δ function in time. In this case, the ground-state wave function has no time to deform, and the excited state appears as a well-localized wave packet. However, real exciting pulses have widths, and, in practice, these are not very different from the time scales of the motion on the potential surfaces. Thus, the discussion of the influence of a finite pulse width becomes an issue of interest.

To be able to answer the questions above, we model the step of initial molecular excitation by a short laser pulse according to Fig. 1. The laser couples the ground state 1 to an excited state 2, so that the energy of the laser photon $\hbar\Omega$ brings the two levels into near resonance at the position of the wave packet; this is shown in the figure by a down shift of the excited state to the dotted potential curve. The coupling allows the resting wave packet to transfer partly to level 2 and start sliding down the slope and away from its position in the ground state. When the laser pulse is over, the transfer ceases and the part excited to level 2 can form the initial state for investigations of the type discussed in [1] and [5]. In contrast to these

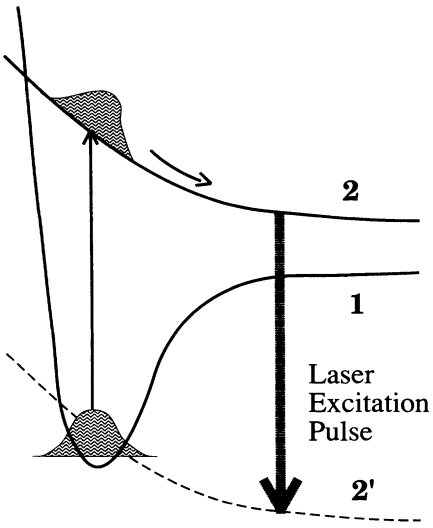

FIG. 1. In our model the laser pulse brings potential surface 2 down to 2' so that it is approximately in resonance with surface 1. As the pulse also couples the surfaces, the initial vibrational wave packet is transferred, at least partly, to surface 2, where it will start to slide down the slope. For simplicity we approximate surface 1 with a harmonic potential, and surface 2 with a linear slope.

works, we cannot utilize the Landau-Zener model for the excitation process discussed here.

In Sec. II, we formulate a mathematical model for the physical situation shown in Fig. 1. In Sec. III, we show how a generalization of the Rosen-Zener model can be used to describe the excitation process, if molecular motion is assumed to play only a minor role. This is the short-pulse limit, and its range of validity is explored by exact numerical integration of the time evolution of wave packets and simple estimates based on the physics of the situation. Two features of the wave-packet evolution lead to finite-time effects; the packet may disperse, or it may move out of the interaction region during the excitation time. The breakdown of the applicability of the generalized Rosen-Zener model is discussed in Sec. IV, where we determine the time range over which the simple approach holds. It turns out that the effects of a finite pulse length can be used to enhance the transfer of population above that predicted by the short-pulse approximation, but then the original smooth wave packet will be distorted and spread out. The outgoing wave packet may be chopped into pieces that leave the excitation region like bullets from a machine gun. These effects are discussed in Sec. V. The paper is concluded by a discussion in Sec. VI.

II. THE FRAMEWORK

We have already discussed how to model complicated, laser-manipulated molecular configurations by a simple system consisting of two crossing potential surfaces with a time-dependent coupling [1,5]. Within the validity of the Born-Oppenheimer approximation, we get the coupled-channel Schrödinger equations

$$i\hbar\frac{\partial}{\partial t}\Psi_1(R,t)=\left[-\frac{\hbar^2}{2m}\frac{\partial^2}{\partial R^2}+U_1(R)\right]\Psi_1(R,t)+V(t)\Psi_2(R,t)\ , \tag{1}$$

$$i\hbar\frac{\partial}{\partial t}\Psi_2(R,t)=\left[-\frac{\hbar^2}{2m}\frac{\partial^2}{\partial R^2}+U_2(R)-\hbar\Omega\right]\Psi_2(R,t)+V(t)\Psi_1(R,t)\ . \tag{2}$$

Here $\Psi_i(R,t)$ are the components of the wave packet $\Psi(R,t)$ that reside on the corresponding electronic energy surfaces $U_i(R)$ (the Born-Oppenheimer, or adiabatic molecular potentials). The vibrational energy resides in wave-packet motion on these surfaces. Therefore, we consider wave-packet transfer between potential surfaces rather than a time-dependent probability redistribution on the discrete quantum-mechanical states. Our system has been simplified further by the assumption of only one relevant nuclear coordinate (one degree of freedom) R.

The laser field at frequency Ω appears as a radiative dipole coupling $V(t)$, and as a shift $\hbar\Omega$ of the potential surface 2 within the rotating-wave approximation. The envelope function $V(t)$ simply reflects the strength and duration of the laser pulse; in the dipole approximation it is a linear function of the laser-field strength. The frequency, duration, intensity, and functional form of the pulse are important factors, especially as they are relatively easy to control externally.

We now insert the system of Fig. 1 into this general framework. Initially ($t\rightarrow-\infty$) the wave packet rests on the ground state of the harmonic potential surface 1 (the lowest vibrational state), so that

$$U_1(R)=\tfrac{1}{2}m\omega^2(R-R_0)^2\ ,$$
$$\Psi_1(R,-\infty)=(2\pi\sigma^2)^{-1/4}\exp\left[-\frac{(R-R_0)^2}{4\sigma^2}+i\phi\right]\ , \tag{3}$$

where $(\Delta R)=\sigma=\sqrt{\hbar/2m\omega}$. The phase factor ϕ is chosen to be such that it cancels the actual time-dependent phase at the particular finite time which we choose as the starting point for the numerical work. If σ is small enough, we can take $U_2(R)$ as a polynomial linear in R:

$$U_2(R)=-\alpha(R-R_0)+\beta,\quad \alpha>0 \tag{4}$$

and we define the detuning $\Delta(R)\equiv U_2(R)-\hbar\Omega-U_1(R)$.

For the laser field amplitude we have chosen

$$V(t)=V_0\,\mathrm{sech}(t/T)\ , \tag{5}$$

where V_0 is the maximum coupling induced by the laser field and T defines the pulse duration. As the two surfaces become coupled by the pulse, a part of the initial wave packet is transferred from surface 1 to surface 2. This transfer is most efficient at the spatial points where the field is in resonance with the potential surface, i.e., where $\Delta(R)=0$. However, the maximum number of these points is only two, and if they are located far from the region of the initial spatial probability distribution [Eq. (3)], the total transfer can become quite small. Evi-

dently, this takes place if $\Delta(R_0)$ becomes very large while α stays small.

Equations (1) and (2) for the system chosen do not appear to be analytically solvable, so we use the numerical method described in the Appendix. We shall shift the spatial coordinate by setting $R_0=0$ and rescale our variables into dimensionless ones:

$$x=\frac{R}{R_c},\quad \tau=\frac{t}{t_c},\quad t_c=\frac{2mR_c^2}{\hbar}\ , \tag{6}$$

so that R_c and t_c are not fixed, but only related. Then, after introducing the scaling

$$\begin{aligned} T_c&=\frac{T}{t_c}\ ,\\ A&=\frac{\alpha t_c R_c}{\hbar}\ ,\\ B&=\frac{t_c}{\hbar}(\beta-\hbar\Omega)=\frac{\Delta(0)t_c}{\hbar}\ ,\\ C&=\tfrac{1}{2}\omega t_c\ ,\\ D&=\frac{V_0 t_c}{\hbar}\ , \end{aligned} \tag{7}$$

we obtain the equations

$$i\frac{\partial}{\partial\tau}\Psi_1(x,\tau)=\left[-\frac{\partial^2}{\partial x^2}+C^2x^2\right]\Psi_1(x,\tau) +D\ \mathrm{sech}\left[\frac{\tau-\tau_0}{T_c}\right]\Psi_2(x,\tau)\ , \tag{8}$$

$$i\frac{\partial}{\partial\tau}\Psi_2(x,\tau)=\left[-\frac{\partial^2}{\partial x^2}-Ax+B\right]\Psi_2(x,\tau) +D\ \mathrm{sech}\left[\frac{\tau-\tau_0}{T_c}\right]\Psi_1(x,\tau)\ , \tag{9}$$

where τ_0 is chosen such that $D\ \mathrm{sech}(\tau_0/T_c)\simeq 0$; in our numerical work we start the integration at $\tau=0$. Now the initial wave packet on surface 1 takes the form

$$\Psi_1(x,0)=\left[\frac{C}{\pi}\right]^{1/4}\exp\left[-\frac{C}{2}x^2\right] \tag{10}$$

with $(\Delta x)=\sigma/R_c=(2C)^{-1/2}$. One can easily see that, as x and τ are dimensionless, so are the parameters defined in Eq. (7). In order to reduce the number of free parameters, we have simply fixed t_c and R_c by using $C=2^{-1/2}$, which gives $t_c=\sqrt{2}/\omega$ and $R_c=(\hbar/\sqrt{2}m\omega)^{1/2}$, but other choices would have been equally possible. We have also mostly confined our studies to those values of B for which $\Delta(R)$ has at least one zero point.

The Schrödinger equations (8) and (9) above form the framework for our numerical investigation of the current problem. However, in the next section we shall discuss how one can utilize the Rosen-Zener model to obtain the transfer probability for cases with very short-pulse durations T_c.

III. THE GENERALIZED ROSEN-ZENER APPROACH

The time-dependent two-state model first studied by Rosen and Zener (RZ) [6] in 1932 is given by

$$i\hbar\frac{\partial}{\partial t}\begin{bmatrix}\Psi_1^{\mathrm{RZ}}(t)\\ \Psi_2^{\mathrm{RZ}}(t)\end{bmatrix}=\begin{bmatrix}\lambda & V(t)\\ V(t) & -\lambda\end{bmatrix}\begin{bmatrix}\Psi_1^{\mathrm{RZ}}(t)\\ \Psi_2^{\mathrm{RZ}}(t)\end{bmatrix}, \tag{11}$$

where λ is a constant and the coupling is $V(t)=V_0\,\mathrm{sech}(t/T)$. If we set $|\Psi_1^{\mathrm{RZ}}(-\infty)|=1$ and $\Psi_2^{\mathrm{RZ}}(-\infty)=0$, we find the solution

$$|\Psi_1^{\mathrm{RZ}}(\lambda,t)|^2=\left|F\left[\frac{V_0T}{\hbar},-\frac{V_0T}{\hbar};\frac{1}{2}-i\frac{\lambda T}{\hbar};z(t)\right]\right|^2, \tag{12}$$

where the time dependence is contained within the function

$$z(t)=\tfrac{1}{2}[\tanh(t/T)+1]\ , \tag{13}$$

and F is the hypergeometric function. For details of the derivation see Ref. [7] or Appendix A of Ref. [8]. When the pulse has died out ($t\to\infty$), one gets from Eq. (12)

$$|\Psi_2^{\mathrm{RZ}}(\lambda,\infty)|^2=\sin^2(\pi V_0T/\hbar)\,\mathrm{sech}^2(\pi\lambda T/\hbar)\ . \tag{14}$$

If we set $\lambda=0$ (so the energy levels are brought into resonance) and define

$$\theta(t)=\int_{-\infty}^{t}dt'V(t')\underset{t\to\infty}{\to}\pi V_0T/\hbar\ , \tag{15}$$

it is easy to obtain

$$|\Psi_2^{\mathrm{RZ}}(\lambda=0,t)|^2=\sin^2\theta(t)\underset{t\to\infty}{\to}\sin^2\pi V_0T/\hbar \tag{16}$$

from Eq. (11). This is known as the area theorem, and the pulse area also appears as a part of the solution (14). The population of the energy levels go through a number of oscillations (Rabi flops) while $V(t)$ is nonzero. Usually the pulse area is defined as $2\theta(\infty)$, so that if $2V_0T/\hbar$ is equal to an odd number, the pulse inverts the level populations, and we call it a π pulse. The optical transparency effect [9,10] takes place when $2V_0T/\hbar$ is an even number (called a 2π pulse by us). Of course, due to absorption, the pulse intensity is changed as it traverses matter, but we assume an optically thin interaction region in order to be able to ignore such effects.

Because of the area theorem we have a way to control the amount of transfer from zero up to a certain value defined by the energy difference of the levels, as seen for the Rosen-Zener case from Eq. (14). We often prefer to choose V_0 and T such that we have a π pulse and therefore expect maximum transfer. When plotting the probability $|\Psi_2^{\mathrm{RZ}}(\lambda,t)|^2$ obtainable from Eq. (12) as a function of time, one can see oscillations which are very much like those anticipated by the area theorem, though reduced in amplitude by the detuning of the levels (see Fig. 2 for an example).

Now, if in our original wave-packet scheme the pulse is extremely short, we can neglect propagation effects during the pulse, i.e., we omit the spatial derivatives in Eqs. (1) and (2) [or in (8) and (9)]. The original wave packet

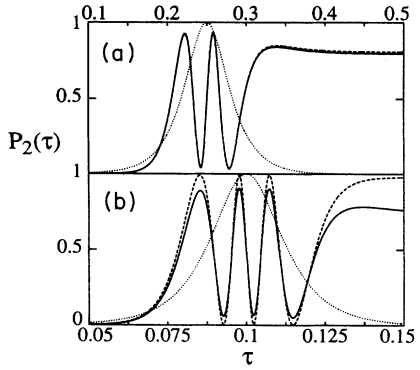

FIG. 2. The time-dependent behavior of the population on the excited potential surface is illustrated here with solid lines, and the corresponding pulse envelope normalized to unity with dotted lines. We have in (a) $A=1$, $B=-12$, $D=100$, and $T_c=0.025$, and (b) $A=50$, $B=10$, $D=350$, and $T_c=0.01$. The dashed line is simply $|\Psi_2^{RZ}(2\lambda=\Delta(0),\tau)|^2$, and in (a) it corresponds quite well with the result of the wave-packet calculation because, for T_c and A suitably small, the Gaussian term dominates the integration in Eq. (19). However, as A is increased, as in (b), deviations occur, although the qualitative behavior holds. We have not plotted $P_2^{RZ}(\tau)$ as the result cannot be distinguished from the wave-packet result $P_2(\tau)$ by eye. In all figures appearing in this paper we have used the value $2^{-1/2}$ for C.

and the potential surfaces are divided into tiny slices over which any variations as a function of position can be neglected. Then we simply apply the Rosen-Zener model with a constant level separation 2λ to each slice. Consequently, for the part of the wave packet residing on surface 2, we get

$$|\Psi_2(R,t)|^2=|\Psi_1(R,-\infty)\Psi_2^{RZ}(2\lambda=\Delta(R),t)|^2 , \quad (17)$$

so each part of the initial spatially distributed wave packet gets transferred to surface 2 independently of the others according to the Rosen-Zener expression, but with the constant energy-level detuning replaced by the spatially dependent potential surface energy difference. We invoke the Franck-Condon principle, which states that nuclear separation R is not altered during a change of electronic quantum state.

With the assumptions above, we obtain the total transfer of population as

$$P_2^{RZ}=\int_{-\infty}^{\infty} dR|\Psi_1(R,-\infty)\Psi_2^{RZ}(2\lambda=\Delta(R),\infty)|^2 \quad (18)$$

$$=\sqrt{C/\pi}\sin^2(\pi DT_c)\times\int_{-\infty}^{\infty} dx\, e^{-Cx^2}\operatorname{sech}^2\left[\frac{\pi T_c}{2}(C^2x^2+Ax-B)\right] . \quad (19)$$

We have defined $P_2(t)$ as the numerical probability transferred to surface 2 in our original model of Sec. II, with $P_2\equiv P_2(\infty)$, and the corresponding Rosen-Zener result is denoted by P_2^{RZ}. Equation (18) becomes time dependent if Eq. (17) is used in the integrand; this defines $P_2^{RZ}(t)$. Naturally, in our scaled units t is replaced by $\tau=t/t_c$.

One should note that the equation above is not limited to our special system (the chosen potential surfaces U_1 and U_2); it could be applied to Morse potentials or to other more realistic cases. On the other hand, the hyperbolic secant pulse shape is one of the few that can be analytically solved for two-level systems. For instance, to the best of our knowledge there are no corresponding results available for the Gaussian or Lorentzian pulse shapes used quite often (see Sec. VI for a discussion).

We have performed the necessary wave-packet calculations and compared them with the corresponding results from the numerical integrations of Eq. (19) and its time-dependent version. Of course, for short π pulses almost all the population is transferred to surface 2. However, in cases where the absolute value of the detuning of the surfaces [$\Delta(x)=-Cx^2-Ax+B$ in our scaled units] exceeds the spectral width of the pulse (proportional to T_c^{-1}) while the initial wave-packet function is still notably nonzero, we may get transfer probabilities clearly less than unity. This situation can be reached by choosing A or $|B|$ large enough compared to T_c^{-1}, although then we move towards the limits where the Rosen-Zener approach breaks down. To cover extensively the full four-dimensional parameter space (A, B, D, and T_c) is a tedious and time-consuming task, so we have just chosen some parameter combinations to check the validity of the Rosen-Zener approach.

In Table I we have examples that illustrate the validity of the Rosen-Zener approach quite well. The data show how P_2 gets smaller as $|B|$ increases. One can notice a hint of the tendency that the approximation gets better with fewer oscillations (first three lines), and is very sensitive to pulse duration (last three lines in Table I). We will discuss the breakdown conditions in greater detail in the next section.

Unfortunately we have been unable to produce an analytic expression for Eq. (19), but any small computer with simple routines can handle it in a reasonable time, unlike the wave-packet calculations which have been performed on a Cray X-MP supercomputer.

In Fig. 2 we have plotted $P_2(\tau)$ with the corresponding $|\Psi_2^{RZ}(2\lambda=\Delta(0),\tau)|^2$. Also, the pulse envelope normalized to unity is displayed. We can see that the correspondence is good in Fig. 2(a) even before integrating over the initial probability distribution; we have chosen $\Delta(0)$ because the distribution has its maximum when $x=0$. However, in the case of Fig. 2(b), the integration is essential, as the hyperbolic-secant amplitude term in Eq. (19) will strongly modify the Gaussian term inside the integral because of the large A.

In Fig. 3 we have plotted the results for π, 2π, and even for $\pi/2$ pulses with different T_c and some different values of A and B. Once again we see the sensitivity to T_c. As T_c increases, we lose both the optical transparency effect (area theorem breakdown) as well as the amplitude approximation (Rosen-Zener envelope breakdown). This breakdown is discussed in the next section.

Note that, in Fig. 3(b), for $A=5$ we have stopped at

TABLE I. Here we have numerical (P_2) results and those obtained from the Rosen-Zener approach (P_2^{RZ}) compared. We have kept $A=3$ and $C=2^{-1/2}$ for all data. The integer part of the pulse area factor DT_c tells us the number of oscillations taking place before the transfer probability settles to its final value.

B	D	T_c	DT_c	P_2	P_2^{RZ}	$\lvert\Delta P_2\rvert/P_2$ (%)
−15	20	0.025	0.5	0.7087	0.7088	0.009
−15	100	0.025	2.5	0.7078	0.7088	0.1
−15	300	0.025	7.5	0.7068	0.7088	0.3
−10	300	0.025	7.5	0.8481	0.8471	0.1
−5	300	0.025	7.5	0.9490	0.9491	0.01
0	300	0.025	7.5	0.9899	0.9899	0.004
5	300	0.025	7.5	0.9606	0.9584	0.2
10	300	0.025	7.5	0.8683	0.8633	0.6
15	300	0.025	7.5	0.7346	0.7285	0.8
−5	350	0.01	3.5	0.9914	0.9914	0.003
−10	150	0.05	7.5	0.5442	0.5576	2.5
−5	75	0.1	7.5	0.4808	0.5583	16

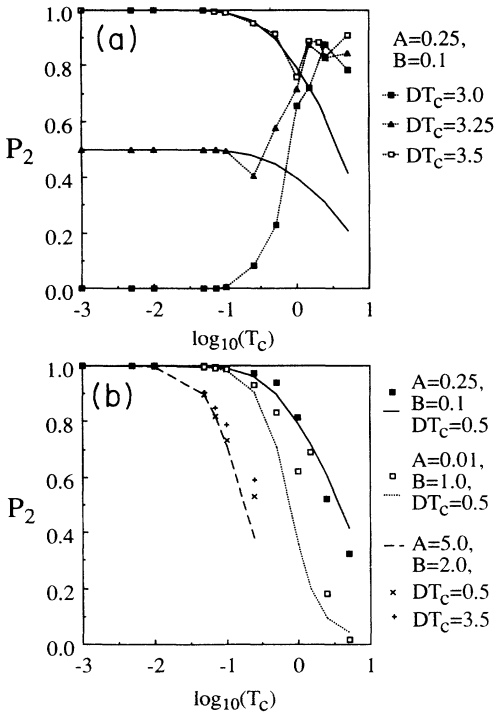

FIG. 3. In (a) of this figure we show the P_2 from the wave-packet calculations (points) compared with the Rosen-Zener result (solid lines). Dotted lines are drawn between the points to guide the eye. The chosen examples are a 2π pulse ($DT_c=3.0$), a $\pi/2$ pulse ($DT_c=3.25$), and a π pulse ($DT_c=3.5$). For small T_c they comply with the area theorem. As T_c increases, the validity of the Rosen-Zener approach breaks down, as well as the area theorem: we find a strong enhancement of transfer, especially in the optical transparency case (2π pulse). In (b) we show the results for three 2π pulses without Rabi flops ($DT_c=0.5$) and for one with them ($DT_c=3.5$). All results seem to follow the corresponding Rosen-Zener calculations (lines) more or less, although deviations clearly increase with T_c. A comparison of (a) and (b) (the $A=0.25$ case) shows that we have an enhancement of population transfer when T_c is large if Rabi flops occur.

$T_c=0.25$ because, for larger T_c, the first excited parts of the packet have time to slide far away from the interaction region. Then the spatial lattice for the numerical calculations must be made quite large to avoid packet reflections from the boundaries, but still dense to maintain the accuracy, which increases the CPU time consumption. This problem might be avoided by assuming absorbing boundary conditions, as has been done, e.g., in Refs. [11,12] (and see also Ref. [13]).

IV. BREAKDOWN OF THE ROSEN-ZENER APPROACH

The Rosen-Zener approach of the previous section breaks down if the population transferred to surface 2 within any slice starts to interfere with that transferred from other slices, or simply move away from the slice region while the coupling is still affecting the system. There are two basic causes for this kind of behavior to appear: (a) if the slope of the surface 2 is steep, parts of the packet start to slide down before transfer is completed, and (b) if T_c is large enough, the dispersion of the transferred wave packet becomes important while the pulse is still on. We can roughly estimate the parameter regions where (a) and (b) give relevant effects.

For surface 2 we get from Ehrenfest's theorem (see [14], p. 41) for the packet acceleration

$$\langle a\rangle=-\frac{1}{m}\left\langle\frac{\partial U_2}{\partial R}\right\rangle=\frac{\alpha}{m}\ , \tag{20}$$

so during the time $\Delta\tau$ the excited part of the packet travels the scaled distance

$$\Delta x=A(\Delta\tau)^2\ , \tag{21}$$

as the mass term is effectively equal to one-half due to our scaling. This distance should be much shorter than the packet width $(\Delta x)_2$ during the pulse duration:

$$AT_c^2\ll(\Delta x)_2\simeq(\Delta x)_{1,0}\ , \tag{22}$$

where the width $(\Delta x)_1$ of the initial Gaussian packet is

used. From here on we use the notation $(\Delta x)_{i,\tau}$ for the packet width on level i at time τ. For our numerical calculations we have fixed $C=1/\sqrt{2}$, so that $(\Delta x)_{1,0}=(2C)^{-1/2}\simeq 0.8409$, and we can write

$$AT_c^2 \ll 1 , \tag{23}$$

as our scaled units are dimensionless. This is the condition for avoiding the sliding effects in our calculations.

For a linear potential, the solutions of the stationary, uncoupled Schrödinger equation are Airy functions [15] with a continuous-energy spectrum. However, here it suffices to consider the motion of the Gaussian minimum uncertainty packet as its dispersion has been treated in detail in Ref. [14], p. 164, and it is the same for a packet on a linear slope (see [16]). The spreading is given by

$$(\Delta x)_{2,\tau}=(\Delta x)_{2,0}\left[1+\frac{\tau^2}{(\Delta x)_{2,0}^4}\right]^{1/2}\simeq\frac{\tau}{(\Delta x)_{2,0}} , \quad \tau \text{ large} \tag{24}$$

and we simply demand

$$T_c \ll (\Delta x)_{2,0}^2\simeq(\Delta x)_1^2\simeq 1 . \tag{25}$$

We shall see later in this paper that the assumptions leading to these limitations are confirmed by numerically obtained values for $\langle x\rangle_2$ and $(\Delta x)_2$.

Consequently, depending on A, the validity of our Rosen-Zener approach is broken because of packet dispersion (small A) or because of packet acceleration (large A). This is intuitively quite clear. In Fig. 4 we show the validity of the Rosen-Zener approach with different values of A and T_c. The lines mark the region where we assume the breakdown to appear. We have defined a "criteria factor" δ so that the solid lines are a combination of $AT_c^2=\delta$ and $T_c=\delta$, whichever condition is first fulfilled as T_c increases. We can see in Fig. 4 how the limits defined above are approached and indeed they seem to hold quite well.

The width of the initial packet is tied to the width of the initial harmonic potential well. Therefore, we do not need to consider the sliding effects of the packet on that surface, as the wave-packet dispersion on surface 2 breaks the validity of the Rosen-Zener approach before these motions become relevant.

There is one more parameter affecting the breakdown, which is somewhat visible already in Table I and in Fig. 3, namely, the number of oscillations (Rabi flops). The transfer probability is not a continuously increasing function of pulse intensity, but an oscillating one. In the crude area-theorem picture we may have full transfer when the envelope has reached only a fractional part of its actual height. Hence, T_c is not the best possible measure for the pulse time scale in the case of intense pulses. However, here we shall concentrate only on cases with less than ten Rabi flops, so we do not take this effect into account but postpone it to possible future studies of intense pulses (see also Sec. VI).

Although wave-packet distortion breaks down the validity of the Rosen-Zener approach, it also introduces quite intriguing behavior in the excited parts of the wave packet, including a so-called machine-gun effect. This will be discussed in the next section.

V. EXAMPLES OF DISTORTED TRANSFER

When the condition (23) for a nonsliding packet is fulfilled, but the dispersion effects are strong, we get the kind of behavior shown in Figs. 5–8. They are examples of cases both with and without the probability oscillations (Rabi flops), as predicted by the area theorem of Sec. III. In Figs. 5(a), 6, and 7, we show the wave-packet characteristics of the nonoscillating case, and Figs. 5(b), 6, and 8 feature the oscillating case with one Rabi flop.

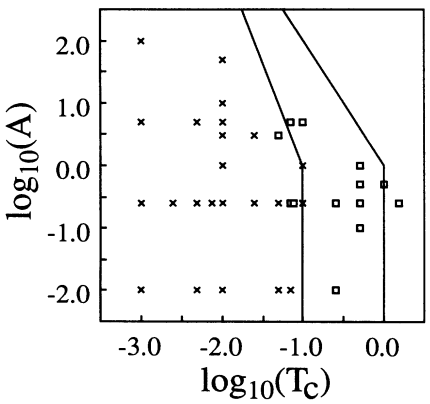

FIG. 4. Here we test the Rosen-Zener approach. To the left of the solid lines we have $AT_c^2<\delta$ and $T_c<\delta$. The first line from the left is for $\delta=0.1$, and the second one for $\delta=1.0$. The crosses mark (T_c, A) combinations for which the relative error $|P_2-P_2^{RZ}|/P_2$ is less than 10^{-3}, and open boxes mark those where this error is larger than 10^{-2}. As the data used here contain pulses with different amounts of Rabi flops, the regions of validity have diffuse boundaries.

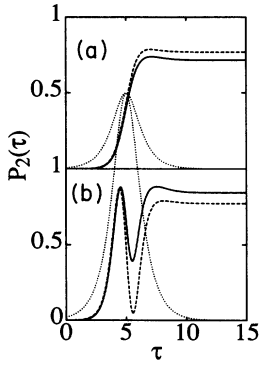

FIG. 5. Here we have $P_2(\tau)$ (solid lines) for (a) the nonoscillating case $D=0.5$ and (b) the oscillating case $D=1.5$, with $T_c=1.0$, $A=0.1$, and $B=0.01$. The dashed line is the corresponding Rosen-Zener result. The wave-packet result first follows the Rosen-Zener result, but then breaks away from it as the packet has had enough time to disperse. In (b) we see how the Rabi flop is partly clipped as excited parts of the packet disperse away from the resonance region [see Fig. 7(b) for a three-dimensional plot]. The dotted lines are the pulse envelopes in our scaled units.

As seen from $\langle x \rangle_2$, in Fig. 6(b), the excited packet indeed slides down surface 2 with the constant acceleration predicted correctly by the classical estimate (20). The anticipated strong dispersion of the excited packet is also clearly visible from $(\Delta x)_2$ of Fig. 6(c). The slope for large τ is linear, as predicted by Eq. (24). However, since the resonance region is narrower than the initial packet, we see that

$$(\Delta x)_{2,0} \simeq 2^{-1/2} = 0.7071 < (\Delta x)_{1,0} \simeq 0.8409 ,$$

as anticipated in Eq. (25).

The propagation of the wave packet in Fig. 7 shows how the excited part spreads rapidly, even climbing up the slope of surface 2, and that only after the pulse is gone does it slowly assume the motion down the slope. Despite the absence of oscillations in $P_2(t)$ in this example, a small part of the packet is transferred back before the pulse dies out [see Fig. 5(a)], resulting in an excited-state "hole" in the region of x where $\Delta(x)$ is smallest.

The part of the packet that remains on surface 1 starts to oscillate with the eigenfrequency of the harmonic potential, as the packet rearranges itself [see Figs. 6(a), 7(a), and 8(a)]. This is connected with the asymmetric population transfer to the higher vibrational states when some of the probability is returned to level 1, but we will not discuss it further in this publication.

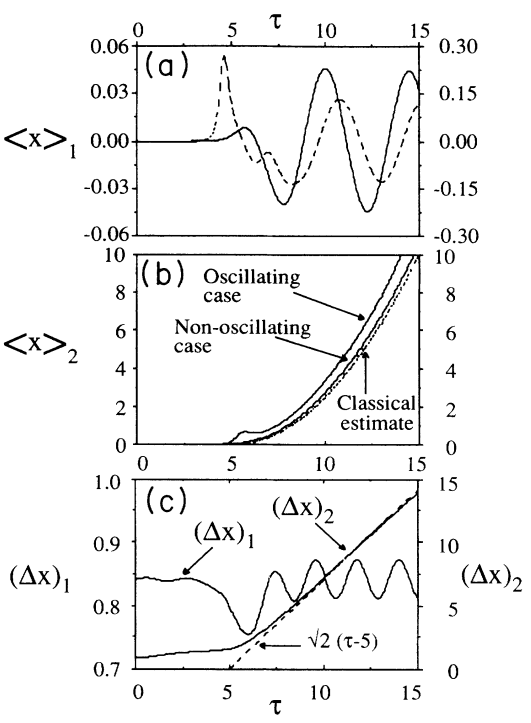

FIG. 6. The main characteristics for the nonoscillating and oscillating cases of Fig. 5 are displayed in this figure. (a) After the pulse, the remnants of the initial packet oscillate with the eigenfrequency of the harmonic potential. This is because the packet is now a superposition of the populations on different vibrational energy states. The solid line and the scale on the left are for the nonoscillating case, and the dashed line and the scale on the right are for the oscillating case. (b) After the pulse, the position of the excited packet behaves quite classically. (c) The packet width in the nonoscillating case shows how the part remaining in the harmonic well oscillates with a frequency twice the eigenfrequency of the well, as can be expected, and the excited part disperses as anticipated in Eq. (24).

Even if the Rosen-Zener method fails to predict the correct P_2 in the example above, the oscillating nature of $P_2(\tau)$ is preserved [see also Fig. 5(b) for another example]. This leads to the effects seen in Fig. 8 as the parts of the excited packet that have not yet dispersed to regions of large $\Delta(x)$ visit surface 1 once more and then return to be dispersed again, finally starting to slide slowly down surface 2.

We can complicate this situation by increasing the slope of the potential surface $U_2(x)$. When A gets larger, condition (23) becomes violated. Then the parts of the excited packet that have dispersed up the slope in the direction of negative x start to return to the region of small $\Delta(x)$ while the pulse is still on. For oscillating cases like those presented in Figs. 5(b) and 8, this actually means that P_2 is reduced as we lose some of the excited population back to surface 1. However, the P_2 obtained still exceeds the Rosen-Zener prediction. Besides, the parts dispersed down the slope are now able to escape faster as A is increased.

If we let A become large enough, dispersion yields its dominance in distortion to the wave-packet acceleration and deceleration due to the steepening of the slope of surface 2. In a case of this kind, we also enhance the final transfer probability P_2 from that predicted by the

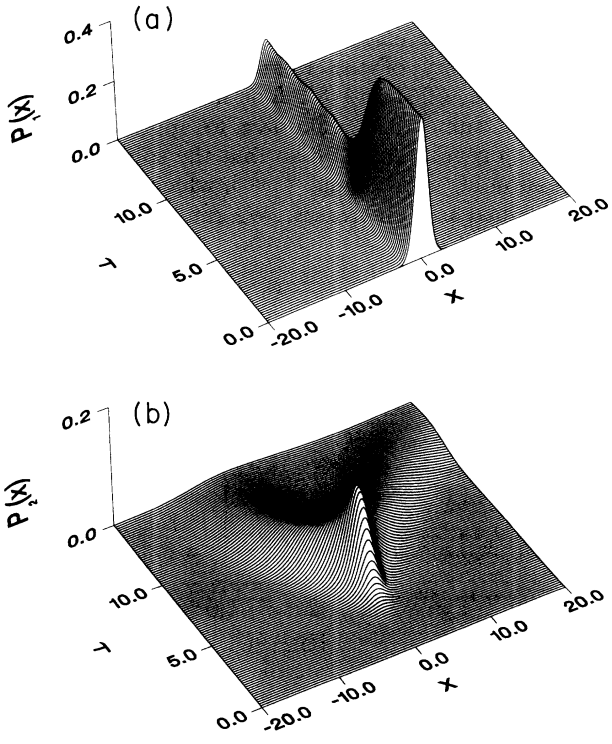

FIG. 7. (a) The depletion and slight oscillations of the packet on surface 1 can be seen here. (b) The excited part of the packet on surface 2 disperses away from the resonance region while the pulse is still on. The parameters are the same as in Fig. 5(a) (the nonoscillating case).

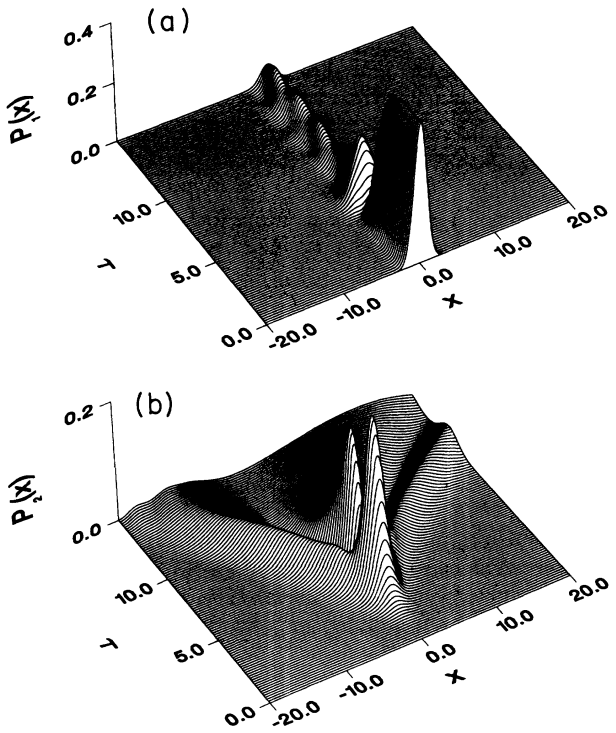

FIG. 8. This figure shows the wave packet for the same parameters as used in Fig. 5(b) (the oscillating case). The small part of excited packet that does not escape the resonance region in time is transferred back to surface 1, and then excited again. (a) This results in oscillations of the packet on surface 1 as more population is distributed to higher vibrational levels. (b) We also see a second peak in the wave-packet structure on surface 2, which starts to disperse and slide down as the pulse dies.

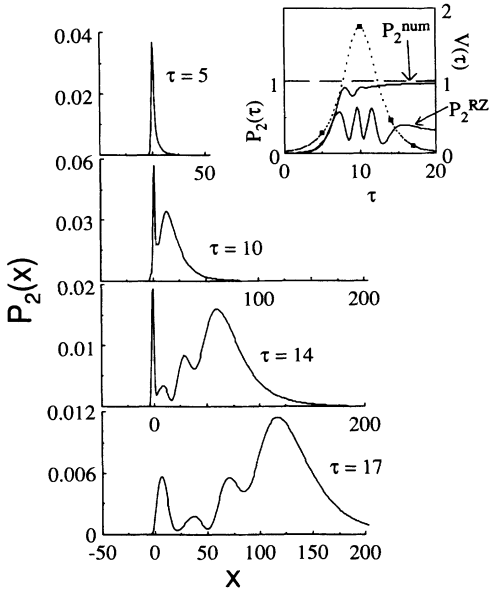

FIG. 10. Here we show the form of the packet on surface 2 at certain times during the excitation and after it. The parameters are $A=1.0$, $B=0.1$, $D=1.75$, and $T_c=2.0$, so that both the dispersion and sliding effects break down the validity of the Rosen-Zener approach. In the upper right corner we have $P_2(\tau)$ (solid lines) and the pulse envelope (dotted line). The snapshots to the left are taken at the points denoted by solid squares in the inset. The Rabi flops in the Rosen-Zener prediction have disappeared from the result of the wave-packet calculation, and by looking at the different τ values we see how the flops form peaks that slide down the slope.

Rosen-Zener approach. Each time an oscillation of $P_2(t)$ reaches a maximum, the transferred part is accelerated away from the interaction region. As seen in Fig. 9, this gradually cuts the oscillations down as A increases. We call this phenomenon the machine-gun effect, as it produces a flow of small peaks in the probability that run down surface 2 like bullets emerging from the crossing region (see Fig. 10). Of course, by increasing D in steps of one we can increase the number of the "bullets in the clip," but then the firing frequency increases and it becomes harder to separate the peaks from each other. Also, there is only a finite amount of probability to distribute to these peaks.

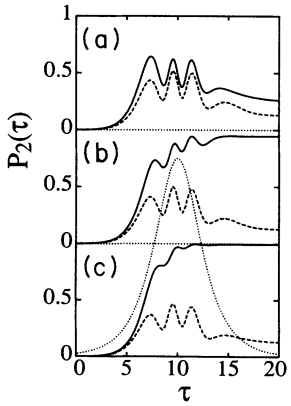

FIG. 9. Here we have $P_2(\tau)$ (solid lines) for $B=1.0$, $D=1.75$, and $T_c=2.0$ with three Rabi flops, and the slope values are (a) $A=0.1$, (b) $A=0.5$, (c) $A=1.0$. We can see how increasing slope A enhances the transfer probability as the oscillations are clipped. This is because the packets are able to escape the interaction region. The dashed lines are the corresponding Rosen-Zener predictions, and the dotted line is the scaled pulse envelope.

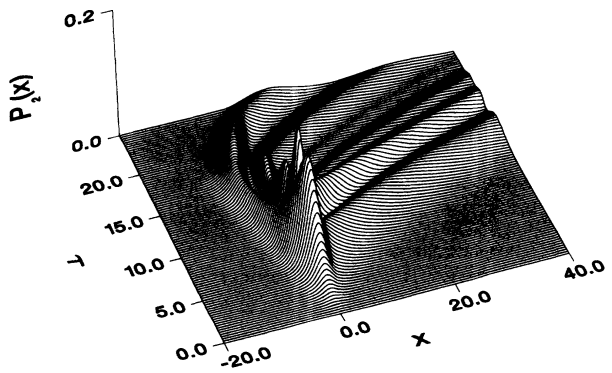

FIG. 11. This figure gives an example where both the sliding and dispersion effects contribute to give a complicated structure to the excited packet. The machine-gun effect is enhanced as parts that have dispersed up the slope start to slide back. Here $A=0.25$, $B=01.$, $D=1.4$, and $T_c=2.5$.

By combining the sliding and dispersion effects, one can modify the machine-gun effect by getting the parts that have dispersed up the slope to contribute to the "ray of bullets" (see Fig. 11 for a good example). This allows one to increase the number of bullets without mixing them too much.

VI. DISCUSSION

In this paper we have not tried to relate our purely theoretical model to any precise physical system which could be, or has been, studied experimentally. The laser intensities needed to achieve some of the effects discussed may be experimentally unrealistic. Our interest has, however, been to investigate the quantum-mechanical characteristics of a model system of coupled potential surfaces and wave packets on them. Of course, as mentioned in the Introduction, the use of ultrashort laser pulses for manipulating and probing of molecular systems is the *primus motor* that triggered this work.

There are several possibilities to extend our theoretical model. The choice of the functional form of the potential surfaces is free because the Rosen-Zener approach [Eq. (18)] requires only that the packet is initially at rest in a bound (stationary) state. The numerical work, however, is not limited by initial conditions; examples of wave packets with nonzero initial momentum were treated in Ref. [1]. There we showed how to probe excited states, and found a good agreement between numerical results and predictions from the Landau-Zener model.

To our knowledge there are no analytical solutions available for the time behavior of a Rosen-Zener type of model with a Gaussian or Lorentzian pulse envelope. In their paper [6], Rosen and Zener conjectured that

$$P_2(\infty)=\left|\frac{\sin A(0)}{A(0)}A(\lambda)\right|^2, \qquad A(\lambda)=\int_{-\infty}^{\infty}dt\,V(t)e^{i2\lambda t}. \tag{26}$$

They anticipated this to be a general solution for all models for an arbitrary nonsingular pulse envelope $V(t)$ and a constant detuning 2λ (nonchirped pulses). Unfortunately, this conjecture is not correct, as shown by Robinson [17], who derives some approximate expressions for Gaussian and exponential pulses.

However, there are several cases of nonsymmetric pulse envelopes whose time-dependent solutions are based on hypergeometric functions [18]. Also, in Ref. [19] Bambini and Lindberg use these nonsymmetric pulses to form symmetric ones that approximate Lorentzian and Gaussian pulse envelopes.

One extension of the model is to use chirped pulses, for which the level structure is time dependent, in addition to the time dependence of the pulse envelope. We have lately paid close attention [8,20] to a hyperbolic secant pulse model, with the Rosen-Zener detuning term λ replaced by $\lambda+E_0\tanh(t/T)$. This model, with a single time scale, was first introduced by Demkov and Kunike in 1969 [7]. For suitable values of λ and E_0 it becomes a level crossing model, like the Landau-Zener model, but with a finite pulse duration. The work of Hioe and Carroll [21] should also be mentioned, and a recent review of pulse models in quantum optics can be found in Ref. [22].

While finishing this study we became aware of the theoretical model by Hill *et al.* [23] for coherent pulse propagation in excimer laser amplifiers. They have the same potential surface structure (harmonic-linear) and initial condition (only the lowest vibrational state is populated), but their approach is different. We study wave packets on potential surfaces, and they discuss state-to-state transfer between quantum-mechanical states. They also concentrate on short but intense pulses with large areas and many Rabi flops, which diminishes the time region where the Rosen-Zener approach is applicable.

As a conclusion we claim that, despite the complexity of molecular systems and their interaction with light, simple analytic models are not yet outdated, but can be applied as long as their shortcomings are recognized. We have found that the Rosen-Zener model can be modified to give predictions on wave-packet transfer between two potential surfaces coupled by an ultrashort pulse, as long as the interaction is short compared to the time scales of packet dispersion and surface structure (packet movement).

ACKNOWLEDGMENTS

The authors thank the Centre for Scientific Computing (CSC) at the Finnish State Computer Centre (VTKK) for access to the Cray X-MP EA supercomputer. One of us (K.-A.S.) acknowledges the financial support of E. J. Sariola Foundation and the Finnish Cultural Foundation/Satakunta Province Foundation.

APPENDIX

This Appendix shows how we have carried out the wave-packet calculations. Although in the actual numerical work we scale the variables and parameters, let us, for clarity, use the original equations (1) and (2), and define

$$T_N=-\frac{\hbar^2}{2m}\frac{\partial^2}{\partial R^2} \tag{A1}$$

as the kinetic-energy operator, and

$$H_{\rm eff}(R,t)=\begin{bmatrix} T_N+U_1(R) & V(t) \\ V(t) & T_N+U_2(R)-\hbar\Omega \end{bmatrix} \tag{A2}$$

as the 2×2 effective Hamiltonian operating on $\Psi=[\Psi_1,\Psi_2]^{\top}$. The solution to the time-dependent problem would then be given by the expression

$$\Psi(R,t_0+\Delta t)=\exp[-i\Delta t H_{\rm eff}(R,t_0)/\hbar]\Psi(R,t_0), \tag{A3}$$

which we expect to be accurate enough for small time steps Δt.

This formal solution is, however, of little use, and like all second-order derivative operators, an application of a forward difference scheme leads to an unstable algorithm. We have used two techniques to overcome this obstacle. A common approach [24] is the Crank-Nicholson

method, which takes the time evolution operator in Eq. (A3) in the form

$$\Psi(R,t_0+\Delta t)=\frac{1-i\Delta t H_{\rm eff}(R,t_0)/2\hbar}{1+i\Delta t H_{\rm eff}(R,t_0)/2\hbar}\Psi(R,t_0)\ . \tag{A4}$$

This expansion is accurate to second order in Δt and has the advantages of numerical stability and manifest unitarity. When Ψ is discretized on a spatial lattice and the denominator in Eq. (A4) is multiplied to the left, we obtain a linear relationship between states at time t_0 and time $t_0+\Delta t$, which can be solved by sparse matrix methods.

The second method used to find the time evolution of Eqs. (1) and (2) is to split $H_{\rm eff}$ into a kinetic part T_N (now a 2×2 diagonal matrix differential operator) and the potential part $W(R,t)$, which covers both the potential surfaces $U_i(R)$ and the pulse coupling $V(t)$. This is called the split operator technique [25,26].

With accuracy to first order in Δt, we can rewrite the operator in Eq. (A3) as a product of the two operators

$$U_T=\exp\left[-\frac{i\Delta t}{\hbar}T_N\right], \tag{A5}$$

$$U_W=\exp\left[-\frac{i\Delta t}{\hbar}W(R,t_0)\right]. \tag{A6}$$

However, second-order accuracy can be obtained by using the symmetrized product $U_W^{1/2}U_TU_W^{1/2}$. Thus, over a time interval Δt, the time evolution in Eq. (A3) can be approximated by

$$\Psi(R,t_0+\Delta t)\simeq U_W^{1/2}(R,t_0)U_TU_W^{1/2}(R,t_0)\Psi(R,t_0)\ . \tag{A7}$$

For many steps this becomes

$$\Psi(R,t_0+n\Delta t)\simeq\left[\prod_{k=0}^{n-1}U_W^{1/2}(R,t_0+k\Delta t)\times U_TU_W^{1/2}(R,t_0+k\Delta t)\right]\Psi(R,t_0)\ . \tag{A8}$$

In order to save time on multiplication steps, we approximate this sequence by

$$\Psi(R,t_0+n\Delta t)\simeq\left[\prod_{k=0}^{n-1}U_W(R,t_0+k\Delta t)U_T\right]\Psi(R,t_0)\ . \tag{A9}$$

This involves replacing $U_W^{1/2}(R,t+\Delta t)U_W^{1/2}(R,t)$ by $U_W(R,t)$ and a small error in the initial and final multiplication by $U_W^{1/2}(R,t)$. For small steps Δt, the errors involved are not expected to be significant.

In general, we have found that the split operator method gives a performance superior to that of the Crank-Nicholson method. The space part U_W is implemented by straightforward multiplication at each point in the spatial lattice, after exact diagonalization of the operator $W(R,t_0)$. The kinetic-energy part is diagonal in the 2×2 matrix indices, but an operator on spatial variables. It is implemented by the introduction of the Fourier transform operator $\mathcal{F}$ defined for an arbitrary function $f(R)$ by

$$\tilde{f}(k)=\mathcal{F}[f]\equiv\frac{1}{\sqrt{2\pi}}\int_{-\infty}^{\infty}dR'e^{ikR'}f(R')\ . \tag{A10}$$

Using this formal operator we can write the kinetic part of the time evolution operator in the form

$$U_T=\mathcal{F}^{-1}\exp\left[-i\Delta t\frac{\hbar k^2}{2M}\right]\mathcal{F}\ . \tag{A11}$$

Numerically we may apply Eq. (A11) by means of a sequence of fast Fourier transforms acting on the discretized wave function. This introduces a finite grid of momentum points, the size of which sets a restriction on the maximum wave-function curvature allowed by the finite lattice spacing introduced in real space. The actual number of discrete points in the spatial lattice used in our numerical calculations was typically 2^{13}.

[1] B. M. Garraway and S. Stenholm, Opt. Commun. **83**, 349 (1991).
[2] M. Gruebele and A. H. Zewail, Phys. Today **43**, 24 (1990).
[3] H. Metiu and V. Engel, J. Opt. Soc. Am. B **7**, 1709 (1990).
[4] S. O. Williams and D. G. Imre, J. Phys. Chem. **92**, 6636 (1988); **92**, 6648 (1988).
[5] B. M. Garraway, K.-A. Suominen, and S. Stenholm, in *Light Induced Kinetic Effects on Atoms, Ions and Molecules,* edited by L. Moi *et al.* (ETS Editrice, Pisa, 1991), pp. 129–138.
[6] N. Rosen and C. Zener, Phys. Rev. **40**, 502 (1932).
[7] Yu. N. Demkov and M. Kunike, Vestn. Leningr. Univ. Ser. Fiz. Khim. **16**, 39 (1969).
[8] K.-A. Suominen and B. M. Garraway, Phys. Rev. A **45**, 374 (1992).
[9] S. L. McCall and E. L. Hahn, Phys. Rev. Lett. **18**, 908 (1967); Phys. Rev. **183**, 457 (1969).
[10] L. Allen and J. H. Eberly, *Optical Resonance and Two-Level Atoms* (Wiley, New York, 1975).
[11] C. Leforestier and R. E. Wyatt, J. Chem. Phys. **78**, 2334 (1983).
[12] R. Kosloff and C. Cerjan, J. Chem. Phys. **81**, 3722 (1984).
[13] R. Heather and H. Metiu, J. Chem. Phys. **86**, 5009 (1987).
[14] E. Merzbacher, *Quantum Mechanics,* 2nd ed. (Wiley, New York, 1970).
[15] L. D. Landau and E. M. Lifshitz, *Quantum Mechanics,* 3rd ed. (Pergamon, Oxford, 1977).
[16] S. Stenholm, in *Quantum Optics, Experimental Gravitation and Measurement Theory,* edited by P. Meystre and M. O. Scully (Plenum, New York, 1983), pp. 117–139.
[17] R. T. Robinson, Phys. Rev. A **27**, 1365 (1983).
[18] A. Bambini and R. R. Berman, Phys. Rev. A **23**, 2496 (1981).
[19] A. Bambini and M. Lindberg, Phys. Rev. A **30**, 794 (1984).
[20] K.-A. Suominen, B. M. Garraway, and S. Stenholm, Opt. Commun. **82**, 260 (1991).

[21] F. T. Hioe and C. E. Carroll, J. Opt. Soc. Am. B **2**, 497 (1985); C. E. Carroll and F. T. Hioe, Phys. Rev. A **41**, 2835 (1990).

[22] B. W. Shore, *The Theory of Coherent Atomic Excitation* (Wiley, New York, 1990), Vol. 1.

[23] K. E. Hill, K. Burnett, and G. H. C. New, J. Mod. Opt. **36**, 965 (1989); K. E. Hill, G. H. C. New, and K. Burnett, J. Chem. Phys. **92**, 5885 (1990); J. Opt. Soc. Am. B **8**, 839 (1991).

[24] W. H. Press, B. P. Flannery, S. A. Teukolsky, and W. T. Vetterling, *Numerical Recipes* (Cambridge University Press, Cambridge, 1986).

[25] J. A. Fleck, J. R. Morris, and M. D. Feit, Appl. Phys. **10**, 129 (1976).

[26] M. D. Feit, J. A. Fleck, and A. Steiger, J. Comput. Phys. **47**, 412 (1982).